The Astrophysical Journal, 705:1139–1151, 2009 November 10 doi:10.1088/0004-637X/705/2/1139

THE EARLY ASYMMETRIES OF SUPERNOVA 2008D/XRF 080109*

Justyn R. Maund[1,2,8], J. Craig Wheeler[3], Dietrich Baade[4], Ferdinando Patat[4], Peter Höflich[5], Lifan Wang[6], and Alejandro Clocchiatti[7]

[1] Dark Cosmology Centre, Niels Bohr Institute, University of Copenhagen, Juliane Maries Vej, DK-2100 Copenhagen Ø, Denmark; justyn@dark-cosmology.dk
[2] Department of Astronomy & Astrophysics, University of California, Santa Cruz, CA 95064, USA
[3] Department of Astronomy and McDonald Observatory, The University of Texas, 1 University Station C1402, Austin, TX 78712-0259, USA; wheel@astro.as.utexas.edu
[4] ESO-European Organisation for Astronomical Research in the Southern Hemisphere, Karl-Schwarzschild-Str. 2, 85748 Garching b. München, Germany; fpatat@eso.org, dbaade@eso.org
[5] Department of Physics, Florida State University, Tallahassee, FL 32306-4350, USA; pah@astro.physics.fsu.edu
[6] Department of Physics, Texas A&M University, College Station, TX 77843-4242, USA; wang@physics.tamu.edu
[7] Departamento de Astronomía y Astrofísica, PUC Casilla 306, Santiago 22, Chile; aclocchi@astro.puc.cl

Received 2009 July 14; accepted 2009 September 21; published 2009 October 19

ABSTRACT

Spectropolarimetry of the Type Ib SN 2008D, associated with the X-ray Flash (XRF) 080109, at two separate epochs, is presented. The epochs of these observations correspond to *V*-band light curve maximum and 15 days after light curve maximum (or 21 and 36 days after the XRF). We find SN 2008D to be significantly polarized, although the largest contribution is due to the interstellar polarization component of $Q_{\rm ISP} = 0\% \pm 0.1\%$ and $U_{\rm ISP} = -1.2\% \pm 0.1\%$. At the two epochs, the spectropolarimetry of SN 2008D is classified as being D1+L(He I)+L(Ca II). The intrinsic polarization of continuum wavelength regions is $< 0.4\%$, at both epochs, implying an asymmetry of the photosphere of $< 10\%$. Similar to other Type Ibc SNe, such as 2005bf, 2006aj, and 2007gr, we observed significant polarization corresponding to the spectral features of Ca II, He I, Mg I, Fe II and, possibly, O I λ7774, about a close-to-spherically symmetric photosphere. We introduce a new plot showing the chemically distinct line-forming regions in the ejecta and comment on the apparent ubiquity of highly polarized high-velocity Ca II features in Type Ibc SNe. The polarization angle of Ca II IR triplet was significantly different, at both epochs, to those of the other species, suggesting high-velocity Ca II forms in a separate part of the ejecta. The apparent structure in the outer layers of SN 2008D has implications for the interpretation of the early-time X-ray emission associated with shock breakout. We present two scenarios, within the jet-torus paradigm, which explain the lack of an apparent geometry discontinuity between the two observations: (1) a jet which punched a hole straight through the progenitor and deposited Ni outside the ejecta and (2) a jet which stalled inside the radius of the photosphere as observed at the second epoch. The lack of a peculiar polarization signature, suggesting strongly asymmetric excitation of the ejecta, and the reported properties of the shock-breakout favor the second scenario.

Key words: supernovae: general – supernovae: individual (2008D) – techniques: polarimetric – techniques: spectroscopic

Online-only material: color figures

1. INTRODUCTION

Core-collapse Supernovae (CCSNe) are inherently asymmetric events, due to the asymmetric nature of the explosion mechanism (see Wang & Wheeler 2008, for a review). Probing the shapes of these events can provide, therefore, important clues as to the nature of the explosion mechanism and its influence on the standard photometric and spectroscopic observables used to measure their properties.

Thomson scattering is a polarizing process, with the polarization of the photon aligned in the direction orthogonal to the plane of scattering (i.e., the plane defined by the ingoing and outgoing photon directions and the point of scattering; Chandrasekhar 1960). In SNe the principal site for this process is at the photosphere, where the opacity is dominated by free electrons. For a resolved spherical photosphere the most significant polarization would be seen to arise from the limb, where only a narrow range of scattering angles (for photons exiting the photosphere and being scattered into the line of sight) are permissible. For an unresolved spherical photosphere, the polarized components arising from regions separated by $\pi/2$ further around the photosphere are equal but opposite, canceling out and leading to a zero net observed polarization. In the presence of asymmetries, there is incomplete cancellation of the polarization components arising from different points in the photosphere, leading to a net observed polarization with the degree of polarization related to the magnitude of the asymmetry and the polarization angle corresponding to the orientation of the asymmetry on the sky (rotated by $\pi/2$). This produces a wavelength-*independent* continuum polarization.

The interaction of continuum photons with the line-forming region also produces a wavelength-*dependent* polarization. Although resonant scattering is inherently depolarizing, absorption along the line of sight removes blueshifted photons (leading to the standard absorption component of P Cygni profiles). If the line-forming region does not equally cover the photosphere, due to some large-scale structure or clumping, then unequal contributions of the polarization components arising from the photosphere will be removed, leading to an increase in polarization across the absorption and the so-called *inverted P-Cygni*

* Based on observations made with ESO Telescopes at the Paranal Observatory, under program 080.D-0107(A).
[8] Sophie & Tycho Brahe Fellow.

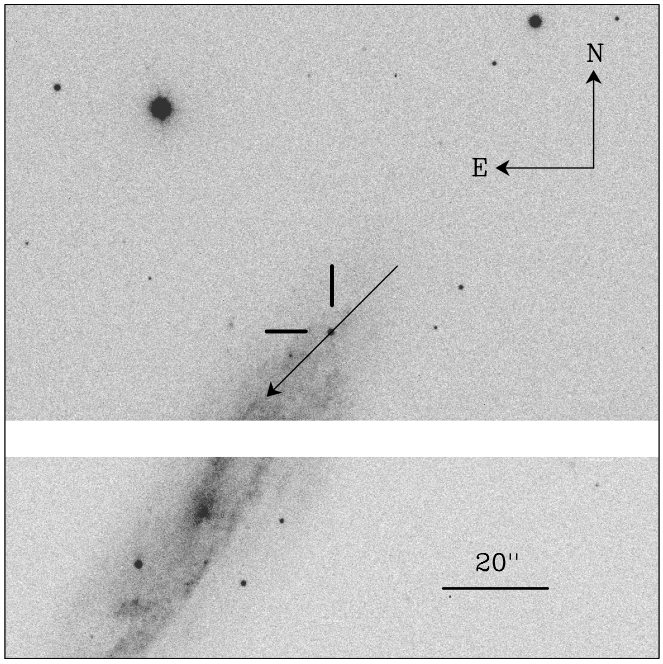

Figure 1. Location of SN 2008D, indicated by the cross hairs, in the galaxy NGC 2770. The direction of the measured ISP component (see Section 4.1) is shown by the arrow. The image is 1 s in the *V* band acquired with the VLT FORS1 and the gap in the image is due to a space between the two detector chips.

profiles in the polarization spectrum (Cropper et al. 1988; Jeffery 1991; Kasen et al. 2003; Höflich et al. 2006). The properties of the polarization at the absorption line are related to the distribution of the line-forming element about the photosphere. Because photons scattered into the line of sight by resonant scattering are depolarized, the redshifted emission components are inherently depolarized. Polarimetry provides, therefore, a unique and powerful way of directly measuring the shapes of SNe at early, optically thick times.

Previous polarimetric studies of CCSNe have shown that the continua of Type Ibc SN are generally more polarized at early times than Type II SNe (Wang et al. 2001; Leonard et al. 2006; Maund et al. 2007a, 2007b, 2007c; Tanaka et al. 2008). In addition, the increase in polarization across the absorption features of P Cygni profiles, coupled with the rotation of the polarization, have demonstrated that the geometries of CCSNe are not described by just a single global axial symmetry (Maund et al. 2007a).

Here we report two epochs of the ESO Very Large Telescope (VLT) spectropolarimetry of the Type Ib SN, associated with the X-ray Flash (XRF) 080109. XRF 080109 was discovered on 2008 January 10 (Berger & Soderberg 2008; Soderberg et al. 2008), in the galaxy NGC 2770, a normal SA galaxy (Thöne et al. 2009). The location of XRF 080109/SN 2008D, relative to its host galaxy, is shown as Figure 1. The XRF was followed by an ultraviolet transient. An associated SN coincident with the XRF was identified (2008D; Li & Filippenko 2008) and was spectroscopically confirmed to be of Type Ib (Soderberg et al. 2008; Malesani et al. 2009; Modjaz et al. 2009). Soderberg et al. (2008) determined that the XRF was non-relativistic, unlike XRFs associated with the gamma-ray burst (GRB) phenomenon, rather arising from the shock breakout arising from an SN explosion. The properties of the XRF suggested it arose from breakout at a radius consistent with a Wolf–Rayet (WR) progenitor star, into a dense wind ($\dot{M} = 10^{-5}\,M_{\odot}$). Mazzali et al. (2008) and Tanaka et al. (2009) modeled the explosion as spherically symmetric, but both found that SN 2008D was only slightly more energetic than normal Type Ibc SNe ($\sim 6 \times 10^{51}$ erg) and less energetic than so-called Hypernovae (e.g., SN 2002ap). Tanaka et al. (2009) found, however, that poor fits of synthetic spectra to observed line profiles indicated the role of significant asymmetries. Here we directly establish those asymmetries by means of spectropolarimetry.

Table 1
Journal of Spectropolarimetric Observations of SN 2008D/XRF 080109

Object	Date UT	Exposure (s)	Median Airmass	Median Altitude	Type
LTT 3218	2008 Jan 31.16	30	1.027	76.74	Flux Std.
SN 2008D	2008 Jan 31.22	8 × 750	1.894	31.80	Object
SN 2008D	2008 Feb 15.18	8 × 900	1.899	31.69	Object
GD 108	2008 Feb 15.23	50	1.056	71.33	Flux Std.
Vela 1 95	2008 Feb 15.24	4 × 30	1.156	59.93	Pol. Std.

The paper is organized as follows: in Section 2 we describe our spectropolarimetric observations of SN 2008D. The results of these observations are presented in Section 3, and these results are analyzed in Section 4. The results and analysis are discussed in Section 5, and we present our conclusions in Section 6.

2. OBSERVATIONS AND DATA REDUCTION

Spectropolarimetry of SN 2008D was conducted at two epochs, 2008 January 31 and 2008 February 15 (corresponding to approximately *V*-band light curve maximum and 15 days after maximum, respectively; Malesani et al. 2009), using the ESO VLT FORS1 instrument in the PMOS mode (Appenzeller et al. 1998). A journal of these observations is shown as Table 1. All observations were conducted with the 300V grism, providing a wavelength range of 3650–9300 Å, and with no order separation filter used. Observations of SN 2008D, at both epochs, consisted of two sets of four exposures at each of the four half-wavelength retarder plate angles. In addition, at each epoch, a flux standard was observed with the full polarimetry optics in place at a single retarder plate angle (0°). The observations were reduced using IRAF[9] and our own specially written software, following the scheme presented by Maund et al. (2007a).

The spectropolarimetric observations at each epoch were combined using a weighted averaging scheme, with the Stokes parameters weighted by the flux. Due to its relatively high declination, SN 2008D was only observed at low altitude (30°) by the VLT. The FORS1 instrument uses a mosaic of two thinned, backside-illuminated 2k×4k E2V CCD44-82 detectors, with increased sensitivity in the blue, but severe fringing and second-order contamination at > 6500 Å (compared to spectropolarimetry with the previous Tektronix CCD detector; e.g., Maund et al. 2007b). The nature of the observations, of a highly reddened object at high airmass with the slit oriented at P.A. = 0° rather than the parallactic angle, was beneficial in that it significantly reduced the flux in the blue (see Figures 2 and 3) and, hence, minimized order contamination of blue flux in the red (and hence contamination of the resulting measured

[9] http://iraf.noao.edu—IRAF is distributed by the National Optical Astronomy Observatories, which are operated by the Association of Universities for Research in Astronomy, Inc., under cooperative agreement with the National Science Foundation.

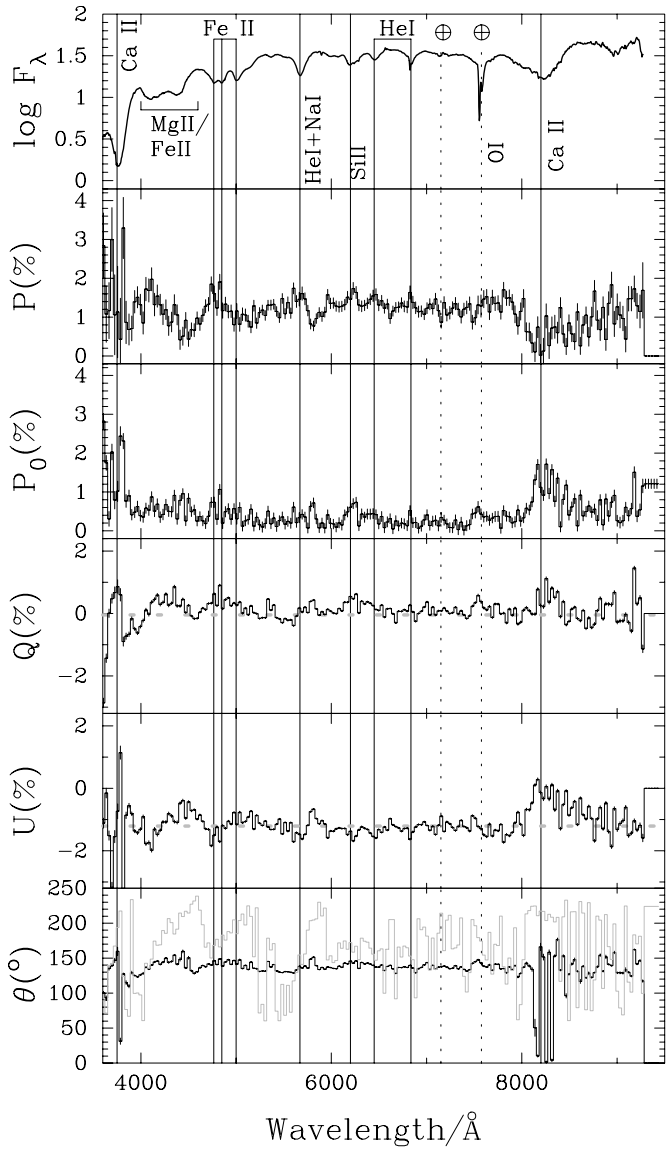

Figure 2. Spectropolarimetry of SN 2008D at 2008 January 31.22. The six panels (from top to bottom) give: the observed flux spectrum, in logarithmic flux units (erg s^{-1} cm^{-2} Å^{-1}), uncorrected for reddening; the observed polarization spectrum (P); the observed polarization spectrum corrected for the ISP (P_0; see Section 4.1); the Stokes Q and U parameters uncorrected for the ISP (the location of the ISP is shown for each panel by the dashed gray line); and the polarization angle θ, uncorrected for the ISP in black and corrected in gray. Line identifications (at absorption minimum) are provided in the top panel, and are based on the identifications of Malesani et al. (2009) and Modjaz et al. (2009). The data are corrected for the recessional velocity of the host galaxy and have been rebinned to 30 Å for clarity.

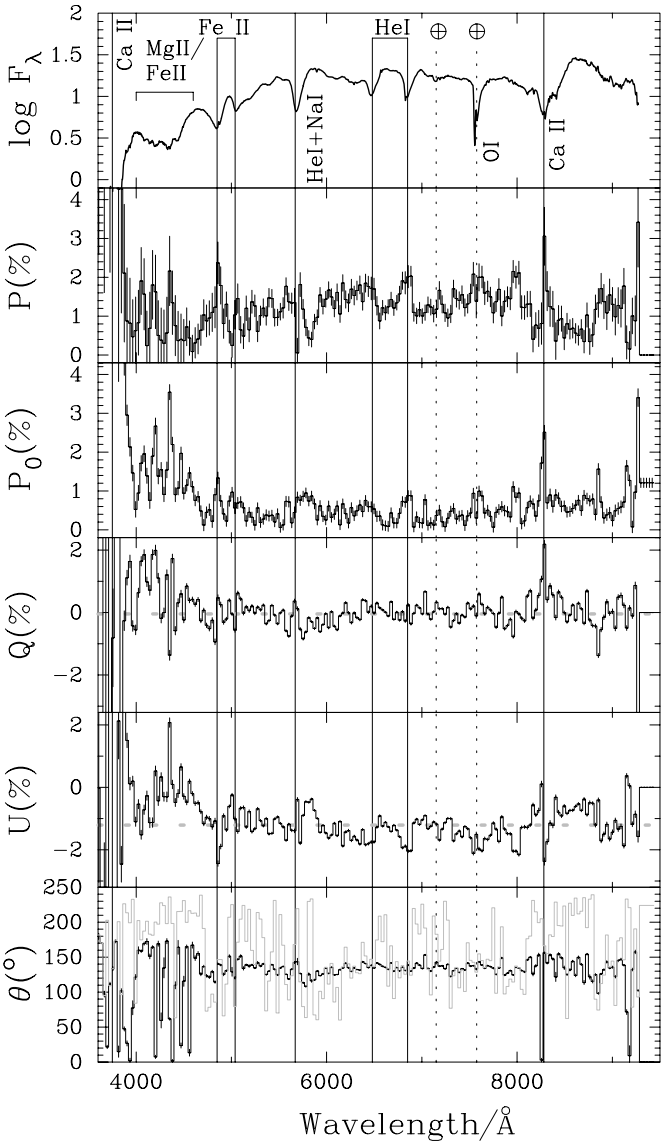

Figure 3. Same as for Figure 2 but for spectropolarimetry of SN 2008D at 2008 February 15.18.

polarization). Since polarimetry uses a relative measurement of flux, the severe reddening of the spectrum has no effect on the final measured degree of polarization.

In order to assess the role of any instrumental changes, including evolution of the fringing pattern, the instrumental signature corrections (ϵ_Q and ϵ_U; Maund 2008) were compared for each pair of data sets and found to be consistent to within the measurement error of $\ll 0.1\%$.

The spectra were flux calibrated, with respect to the observed flux standard, but were *not* corrected for atmospheric extinction (such that the flux spectra presented here are significantly redder than presented elsewhere). The calibration of the PMOS mode of FORS1 was checked using observations of the polarized standard star Vela 1 95. The data were corrected for the heliocentric recessional velocity of the host galaxy of 1947 km s^{-1}.[10]

Synthetic broad V-band polarimetry was measured from the data, weighting the observed spectropolarimetry as a function of wavelength with the Johnson V passband response function.

3. OBSERVATIONAL RESULTS

The observed spectropolarimetry of SN 2008D at 2008 January 31 and 2008 February 15 is presented in Figures 2 and 3.

3.1. General Spectroscopic Properties

We summarize the spectroscopic properties of SN 2008D at the two epochs of our observations, to serve as an orientation for the discussion of the polarimetric properties of this object. Previously, spectra of SN 2008D have been presented by Soderberg et al. (2008), Malesani et al. (2009), Modjaz et al.

[10] NED: http://nedwww.ipac.caltech.edu

(2009), Mazzali et al. (2008), and Tanaka et al. (2009). Here we adopt the line identifications made by Malesani et al. (2009) and Modjaz et al. (2009).

At the two epochs of our observations the spectrum of SN 2008D is composed of broad P Cygni profiles of He I, Ca II, O I, and Fe II.

Ca II H&K and the IR triplet (IR3) are present at the blue and red extremes of the spectra. At the first epoch, the full P Cygni profile of Ca II H&K is observed, with the absorption minimum at −14,100 km s^{-1}. In addition, weak narrow absorptions are also observed superposed on the emission feature, at the rest wavelength in the host galaxy, arising in the interstellar medium. At the second epoch, the absorption component is no longer detected, due to the spectrum becoming redder and steeper, such that only the emission component and the decline toward the minimum are observed. The Ca II IR3 feature is detected at both epochs. At the first epoch, the emission component is truncated in the red by an O I line (Modjaz et al. 2009). The absorption component, corresponding to a velocity of −12, 000 km s^{-1}, is a broad single-minimum feature. At the second epoch there is little evidence of the redward absorption due to O I, but the absorption minimum of Ca II IR3 is separated into seemingly high-velocity (HV) and low-velocity minima at −10, 200 km s^{-1}and −6400 km s^{-1}, respectively (but note that the HV component is moving at lower velocities than the single component observed at the first epoch).

Similar to the spectrum of SN 2005bf, Fe II (42) is observed as separate resolved absorption minima at the first epoch ($v \sim$ 9500 km s^{-1}); at the second epoch, due to a general decrease in observed velocities the Fe II features are blended into a single profile, with a likely significant contribution from He I λ5015, commensurate with the observed increase in the strength of other He I lines elsewhere in the spectrum. A combined Mg II λ4471 and Fe II(37,38) feature is observed at ∼4400 Å.

At the first epoch a set of He I lines (λλ5876, 6678, 7065) are observed in the spectra, with the two redder lines being observed as slight notches (corresponding to $v_{\rm He} = -10{,}100$ km s^{-1}). The stronger He I λ5876 line may also be blended with Na I, which may explain the apparent disparity between line strengths in the He I series. At the second epoch the He I lines have significantly increased in strength, although with a slight decrease in velocity to −9500 km s^{-1}. A narrow absorption is observed at the rest wavelength of Na I D at the host galaxy.

At the first epoch, Si II λ6355 is observed as a shallow P Cygni profile, that is potentially blended with a high-velocity component of Hα (Malesani et al. 2009). Assuming this feature is purely due to Si II the absorption minimum corresponds to −7790 km s^{-1}. This feature is absent from the data of the second epoch. There is a hint of O I λ7774 in emission, with the corresponding absorption trough coincident with the nearby telluric feature (suggesting an approximate velocity $\sim -$ 8000 km s^{-1}at the first epoch, and $v \sim$ 7600 km s^{-1} at the second). Modjaz et al. (2009) observe the full P Cygni profile of the O I line in their spectroscopic data, at 2 days prior to our first observation.

The Galactic foreground reddening to SN 2008D is given as $E(B-V)_{\rm MW} = 0.023$ (Schlegel et al. 1998). The equivalent width of Na I D measured from our low-resolution data is a poor indicator of reddening arising in the host, as previous high-resolution studies of SN 2008D have shown it to be a superposition of a number of different, saturated absorption systems (Soderberg et al. 2008; Modjaz et al. 2009). Previous studies have determined the reddening to fall in the range

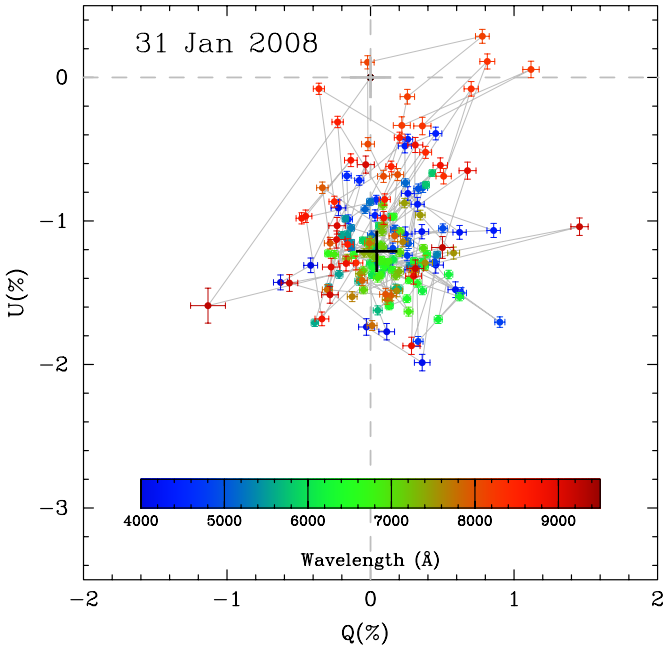

Figure 4. Spectropolarimetry of SN 2008D at 2008 January 31.22 on the Stokes *Q–U* plane, uncorrected for the ISP. The location of the ISP is indicated by the black cross, and the zero polarization is indicated by the gray cross and dashed lines. The observed data are color coded according to wavelength, following the scheme in the color bar.

(A color version of this figure is available in the online journal.)

$E(B-V) = 0.6$–0.9 (Soderberg et al. 2008; Malesani et al. 2009; Modjaz et al. 2009; Mazzali et al. 2008; Thöne et al. 2009). Here, we adopt the value $E(B-V) = 0.65$, the most commonly used value, and assume the foreground reddening is negligible.

3.2. General Spectropolarimetric Properties

The spectropolarimetric data are plotted on the Stokes *Q–U* plane for both epochs in Figures 4 and 5. SN 2008D is observed to be significantly polarized at both epochs, with a baseline polarization of $P \sim 1.3\%$. As shown in Figures 2 and 3, this level of polarization is common at both epochs. Most of this polarization is in the *U* Stokes parameter, as evident in Figures 4 and 5, as the data points are clustered in the same location of the Stokes *Q–U* plane and the polarization angle is ∼135° across most of the spectrum. The apparent rise in the polarization at the blue and red extremes of the data is consistent with an increase in the uncertainties on the measured polarization, due to declining signal to noise in these portions of the spectrum and the possible wavelength dependence of the interstellar polarization (ISP).

The most significant deviations from this baseline level of polarization are associated with spectral features. At the first epoch a peak polarization of $3\% \pm 0.8\%$ is observed at the Ca II H&K absorption component. This is contrasted for the Ca II IR3 absorption, for which the absorption minimum is associated with a minimum (0.6%) in the polarization spectrum. On the *Q–U* plane, the data corresponding to the Ca II IR3 absorption are observed to lie distinctly separate from the rest of the data. Significant polarization is associated with the He I λ5876 line, and the redder He lines are also polarized albeit at a lower degree. With the increase in the strength of the He I lines at the second epoch, there is a correlated increase in the polarization. The resolved absorption components of the Fe II(42) multiplet

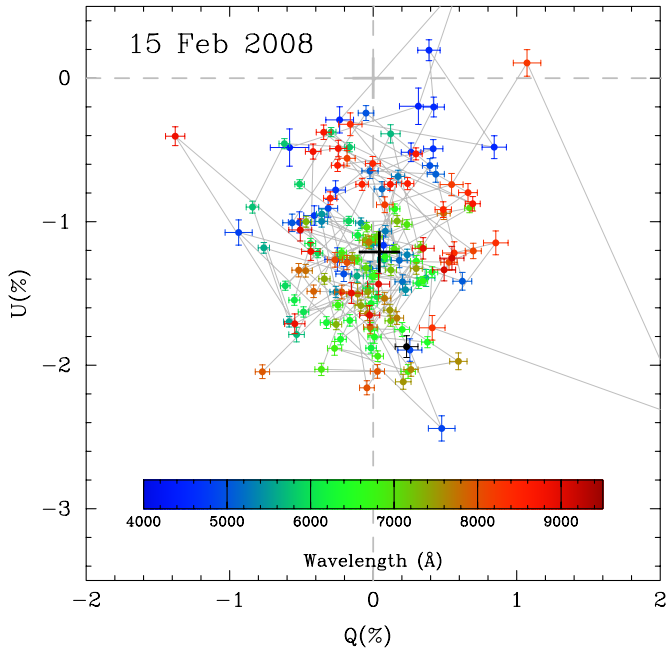

Figure 5. Same as for Figure 4, but for spectropolarimetry of SN 2008D at 2008 February 15.18.

(A color version of this figure is available in the online journal.)

and the Mg II λ4471 line, at the first epoch, are associated with strong polarization at the level of 1.8% ± 0.2%.

Given the substantial degree of reddening associated with this SN (see Section 3.1), there is the expectation that the ISP component is non-zero. As has been demonstrated in a number of cases, the determination and subtraction of the ISP component is vital to determining the intrinsic polarization (P_0) and, hence, geometry of SNe. Importantly, the ISP can cause intrinsically unpolarized features to be observed to be polarized and make polarized features appear depolarized. The standard expectation for P Cygni profiles, in the flux spectrum, is that significant polarization is associated with the absorption component while the emission component is unpolarized. We see that, at the first epoch, the absorption component of Ca II IR3 is unpolarized. Furthermore, we note that the general behavior of the data on the Stokes Q–U plane is constant with time, occupying the same location (despite variability in the polarization associated with spectral lines).

Synthetic V-band polarimetry of this data yielded $p_V = 1.2\% \pm 0.1\%$ ($\theta = 135°$) and $1.1\% \pm 0.1\%$ (131°), at 2008 January 31 and 2008 February 15, respectively. Gorosabel et al. (2008) present broad V-band polarimetric measurements which, not only agreeing with our synthetic V-band polarimetry, also show that SN 2008D occupies the same location of the Q–U plane prior to and following our two observations (see Section 5).

4. ANALYSIS

4.1. Interstellar Polarization

The determination of the ISP is crucial to determining the intrinsic polarization of the SN. The reddening toward SN 2008D can be used to provide a constraint on the maximum degree of ISP. The total reddening to SN 2008D (see Section 3.1) constrains the ISP to be $p_{\rm ISP} < 5.85\%$ (assuming a standard Serkowski-Galactic type ISP), arising predominantly in the host galaxy. In order to make a precise estimate of the ISP component particular assumptions must be used, principally based on there being portions of the spectrum that are intrinsically unpolarized, such that the observed polarization of these regions is due to the ISP alone. We attempt to remove only a single total ISP, rather than account for individual ISPs arising in the Galaxy and the host galaxy, as the total ISP is a vector sum of all individual components. A number of techniques, based on this primary assumption, have been used and we discuss in turn the alternative values of the ISP indicated.

Under the assumption that particular wavelength regions of the spectrum are intrinsically depolarized due to the blending of numerous overlapping Fe lines in the range 4800–5600 Å, Howell et al. (2001) used the observed polarization properties at particular wavelengths as measures of the ISP. The Fe II multiplet 42 lines are clearly resolved at both epochs (Maund et al. 2007a), however immediately redward in the range 5200–5500 Å there are a number of overlapping features. Under the assumption that the line blanketing opacity dominates over electron scattering in this wavelength range, such that this region is intrinsically depolarized, we measure the median average values of the Stokes parameters as $Q_{\rm ISP} = -0.085\% \pm 0.234\%$ and $U_{\rm ISP} = -1.164\% \pm 0.175\%$ at the first epoch and $Q_{\rm ISP} = -0.061\% \pm 0.240\%$ and $U_{\rm ISP} = -1.164\% \pm 0.266\%$ at the second epoch. These values of the ISP Stokes parameters are identical, within the uncertainties, and the average value corresponds to $p_{\rm ISP} = 1.16\% \pm 0.15\%$ and $\theta_{\rm ISP} = 133° \pm 4°$.

An additional measurement can be derived using the technique of Tran et al. (1997), under the assumption that the emission component of a P Cygni profile is intrinsically unpolarized. The polarization of the emission component, corrected for the polarization of the continuum (actually a mixture of the intrinsic continuum polarization and the ISP), reflects the ISP component alone and can be measured by a least-squares fit to the equations $Q_{\rm tot} \times F_{\rm tot} = Q_{\rm cont} \times F_{\rm cont} + Q_{\rm line} \times F_{\rm line}$ and $U_{\rm tot} \times F_{\rm tot} = U_{\rm cont} \times F_{\rm cont} + U_{\rm line} \times F_{\rm line}$ to determine the Stokes parameters of the emission line $Q_{\rm line}$ and $U_{\rm line}$ (in the presence of no ISP $Q_{\rm line} = U_{\rm line} = 0$). This technique was applied to the emission components of the Mg I λ4470/Fe II and Ca II IR3 lines at the second epoch, where a good approximation for the continuum level could be made. At the first epoch, the emission components of these lines are truncated by blends with other features, whereas at the second epoch these features appear unblended. The ISP component was measured for both lines to be $Q_{\rm ISP} = 0\% \pm 0.1\%$ and $U_{\rm ISP} = -1.3\% \pm 0.1\%$ (where the quoted error is the scatter in fits using different wavelength ranges and different continuum levels).

The fact that the ISP is time-invariant supports these values, given the apparent constant level of polarization and the constant location of the data on the Q–U plane at the two observational epochs. Gorosabel et al. (2008) observed similar Stokes parameters with their broadband polarimetry, between 3.6 and 78.5 days post-explosion, suggestive that the bulk of the observed polarization (excluding polarization associated with strong lines) was due to a unvarying ISP.

In general, the ISP is expected to be wavelength-dependent, but characterizing this dependence is difficult for objects such as SN 2008D which show strong intrinsic wavelength-dependent polarization associated with spectral lines. For a Serkowski-type ISP, for Milky Way-like dust, the difference in ISP between the peak polarization, at a characteristic wavelength of 5500 Å, and the ISP polarization measured for the emission components of

the Ca II lines at the blue and red ends of the spectrum is smaller than the error of the measured Stokes parameters of the ISP. The small degree of wavelength dependence justifies the use of a single-valued, wavelength-independent ISP as inferred from these data. For a number of SNe, the wavelength-dependence of the ISP, arising from their host galaxies, has been observed to deviate significantly from a standard Serkowski et al.-type ISP law (Leonard & Filippenko 2001; Maund et al. 2007a; Patat et al. 2009). In the case of SN 2008D, there is no evidence for the magnitude of the polarization rising significantly at either the blue or red extremes of the observed spectrum (suggesting the peak in the ISP occurs within the wavelength range of these observations). In fact, the baseline polarization of the data is approximately constant across the observed wavelength range, with a possible peak around 5500 Å (see above), which lends further credence to the to the assumption that the ISP can be considered approximately wavelength-independent for our observations (with any wavelength dependence of the ISP over the wavelength range being smaller than the uncertainties of our wavelength-independent estimate).

The weighted average of the measured Stokes parameters for the ISP, from the different methods, are $Q_{\rm ISP} = -0.04\% \pm 0.13\%$ and $U_{\rm ISP} = -1.21 \pm 0.12$, which correspond to $p_{\rm ISP} = 1.21\% \pm 0.12\%$ and $\theta_{\rm ISP} = 134^\circ \pm 4^\circ.3$. The direction of the ISP vector is shown in Figure 1. Contrary to the standard prediction that the ISP vector be aligned with the spiral arms of the host galaxy, due to the alignment of dust grains by magnetic field lines parallel to the spiral arm (Scarrott et al. 1987), the ISP is not aligned with the nearest spiral arm. This may indicate that the ISP determined may either be incorrect, that the magnetic field in the host is not aligned with the spiral arms at large radii or that the ISP is the sum of a number of separate components, perhaps arising in the Galaxy, the host galaxy, the intervening medium and, importantly, in the circumstellar environment of the SN.

4.2. The Intrinsic Polarization of SN 2008D

4.2.1. The Continuum

After correcting the observed data for the ISP, we note that away from obvious spectral features the intrinsic polarization is generally $< 0.4\%$. Furthermore, at both epochs the wavelength region 7100–7500 Å appears to have a relatively constant low polarization, with only weak features appearing in the flux spectrum. Using this region as representative of the continuum, we measure the intrinsic polarization to be $0.22\% \pm 0.14\%$ and $0.21\% \pm 0.17\%$ at the first and second epochs, respectively (where these values are weighted means over the data in this wavelength range). Assuming a spheroidal photosphere, this polarization corresponds to an apparent axial ratio > 0.9 (Höflich 1991).

4.2.2. He I λλ5876, 6678, 7065

Significant intrinsic polarization is associated with the He I lines at both epochs. At the second epoch, higher levels of polarization are measured for the redder He I lines, in line with the absorption becoming stronger (i.e., the fraction of continuum photons being removed by the line is larger at the second epoch). If the line-forming region, for a general line, blocks all the unpolarized light from a spheroidal photosphere, then the maximum degree of polarization expected at absorption minimum ($p_{\rm trough}$) is

$$p_{\rm trough} \leqslant p_{\rm cont} \cdot \frac{F_{\rm cont}}{F_{\rm trough}} \quad (1)$$

following the prescription of Leonard et al. (2002), where $p_{\rm cont}$ is the degree of polarization measured in adjacent "continuum" regions and $F_{\rm cont}$ and $F_{\rm trough}$ are the fluxes measured at the nearby continuum and at the absorption component minimum, respectively. There is some difficulty with the measurement of the maximum polarization of He I λ5876 in the intrinsic polarization spectrum, as there is variability at and around the position corresponding to the absorption line minimum in the flux spectrum. We note, however, that the redder He I lines show the expected inverted P-Cygni profile in the polarization spectrum. At the second epoch, for λλ5876, 6678, 7065 we estimate theoretical polarization limits of 0.68%, 0.44%, and 0.45%, respectively, as opposed to the observed values of 1.11%, 0.58%, and 0.73%. Leonard et al. (2001, 2002) and Tanaka et al. (2008) present a number of reasons why this theoretical limit may not be actually observed: depolarization of resonantly scattered continuum photons in optically thick lines, the contribution of strong emission line components or clumpy ejecta.

A significant clue as to the true reason behind the significant polarization is observed in the rotation of the polarization angle across the He I λ5876 line (and to a lesser extent for λλ6678, 7065). This rotation corresponds to a velocity-dependent loop structure, which is shown in Figure 6. Such a loop feature is generally interpreted as a departure from a single global axial symmetry, such that the axis of symmetry of the line-forming region is not aligned with that of the photosphere and the line-forming region also only covers a fraction of the photosphere (Kasen et al. 2003; Maund et al. 2007a). The similarity

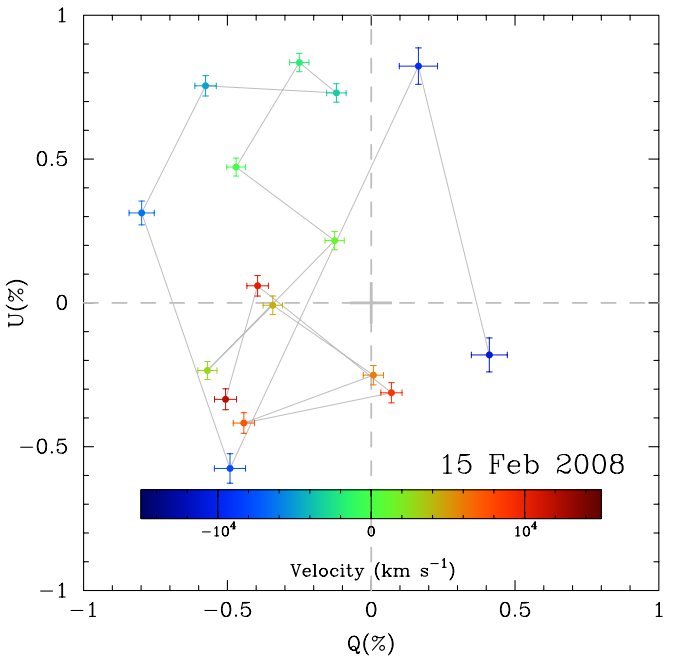

Figure 6. Polarization across the He I λ5876 line at 2008 February 15. The points are color coded according to velocity with respect to the rest wavelength of the line. The data have been corrected for the recessional velocity of the host galaxy and the ISP. The data marked in blue correspond to the polarized absorption component of the line profile.

(A color version of this figure is available in the online journal.)

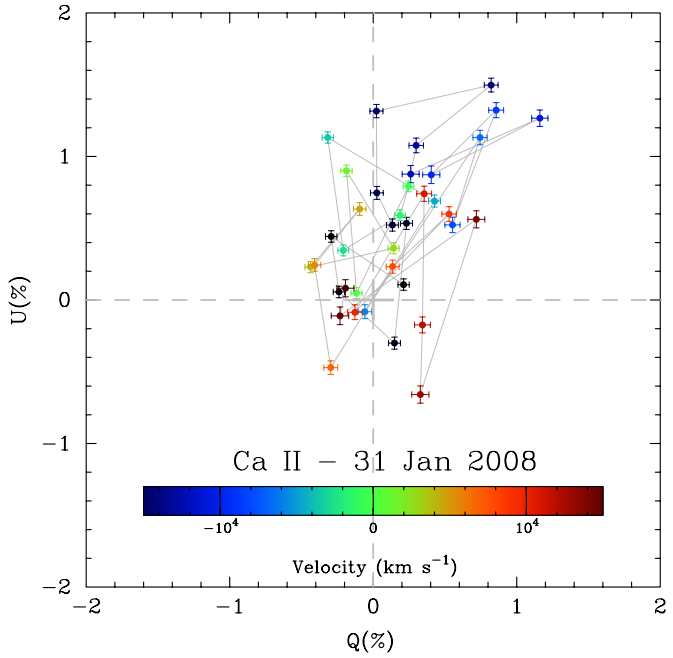

Figure 7. Same as Figure 6 but for the Ca II IR3 feature at 2008 January 31. (A color version of this figure is available in the online journal.)

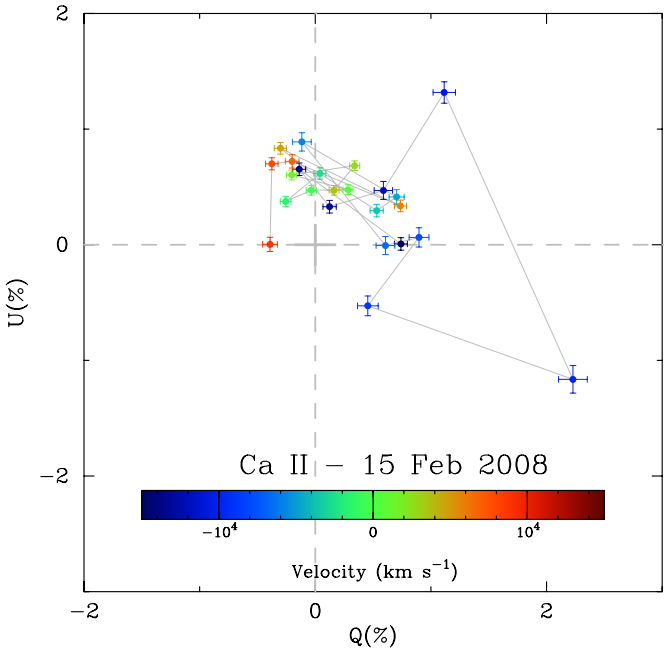

Figure 8. Same as Figure 6 but for the Ca II IR3 feature at 2008 February 15. (A color version of this figure is available in the online journal.)

of the polarization angle of three He I lines, $\theta_{5876} = 141° \pm 9°$, $\theta_{6678} = 147° \pm 9°$, and $\theta_{7065} = 152° \pm 7°$, at the first epoch suggests a common geometry for the line-forming regions of these lines. The two red He I lines have similar polarization angles at the second epoch, $\theta_{6678} = 147° \pm 7°$ and $\theta_{7065} = 154° \pm 5°$, suggesting the He I line-forming region is the same as in the first epoch. The polarization angle associated with He I λ5876 changes to 39° ± 7°, suggesting possible blending due to Na I D.

At the second epoch, He I λ5015 is also expected to be a prominent feature, although coincident with a number of Fe II lines. The presence of this line is suggested by the similar polarization angle (147° ± 6°) associated with the absorption at 4890 Å.

We conclude that the violation of Equation (1) and the observed rotation of the polarization angle for the He I lines is due to the lines arising in an excited He I clump that is off-axis relative to the axis of symmetry of the photosphere and does not cover the full area of the photosphere.

4.2.3. Ca II

At the first epoch, Ca II H&K is observed to be polarized (with an inverted P-Cygni profile) at 2.4% ± 0.8%, a similar level to that observed for the Ca II IR3 at 1.8% ± 0.3%. The Ca II IR3 absorption feature is observed to be polarized at both epochs, with the subtraction of the ISP, producing the expected "inverted P-Cygni profiles" in the polarization spectra. As it is unclear if the flux at the absorption minimum of the Ca II H&K feature is significantly detected at the second epoch (Section 3.1), we cannot ascertain the real degree or significance of the observed polarization around the wavelength of that feature at that epoch. At the second epoch, in which a probable HV component is observed, a polarization of Ca II IR3 is observed to be 2.5% ± 0.7%. This suggests the apparent HV component at the second epoch also produces the absorption minimum at the first epoch, and the two components were not resolved at the first epoch. Similarly to Section 4.2.2, the theoretical limiting polarization for Ca II is 0.92%, such that the observed data suggest a similar scenario for Ca II (as suggested for He I) being formed in a region with a different axial symmetry to that of the photosphere and incomplete coverage. At the first epoch the polarization angle at the Ca II IR3 absorption minimum is 37° ± 4°, whereas at the second epoch the angle is 25° ± 3°. Importantly, these angles are significantly different than those observed for He I, O I, and Fe II, suggesting the Ca II IR3 line forms in a significantly different portion of the ejecta to the lines of the other species.

At the first epoch, the absorption component of IR3 is obviously polarized, although the data are not of sufficient quality (due to the severity of fringes) to discern a loop (see Figure 7). By the time of the second epoch, a loop is easily identified (Figure 8) corresponding to the HV component of the absorption profile.

4.2.4. Fe II

The observed level of polarization associated with the Fe II(42) lines is significantly reduced upon subtraction of the ISP, as indicated in Figures 2 and 3. Some polarization is still associated with these lines at the first epoch (0.6%–1% ± 0.2%), but a larger polarization (1% ± 0.3%) is observed at this wavelength at the second epoch, due to the increase in strength of the He I λ5015 line (see Section 4.2.2).

At the first epoch, the peak polarization for the bluest absorption of Fe II(37,38), at −9600 km s^{-1}, is 0.9%. Another polarization peak at 1% is observed at 4441 ± 15 Å, without an obvious counterpart in the flux spectrum. It may correspond to the 4584 Å line, in the same multiplet, at the velocity determined above.

4.2.5. O I

A weak polarization signature is associated with O I λ7774 measured to be 0.50% ± 0.13% at 17° ± 18° and 0.3% ± 0.13% at 155° ± 4°, at the first and second epochs, respectively. The large errors are due to the coincident telluric

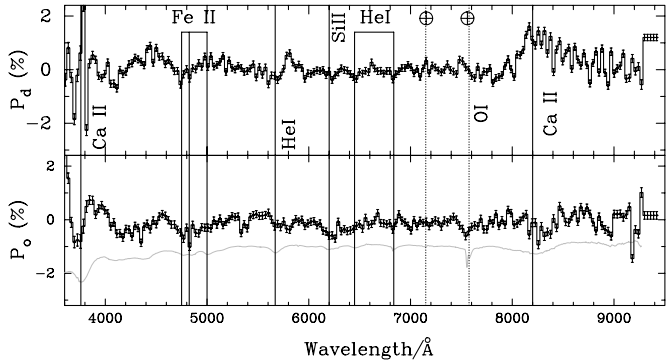

Figure 9. Spectropolarimetry of SN 2008D at 2008 January 31.22, projected onto the dominant (P_d; top panel) and orthogonal (P_o; bottom panel) axes. For comparison, the flux spectrum is plotted in gray in the bottom panel. Line identifications are those from Figure 2.

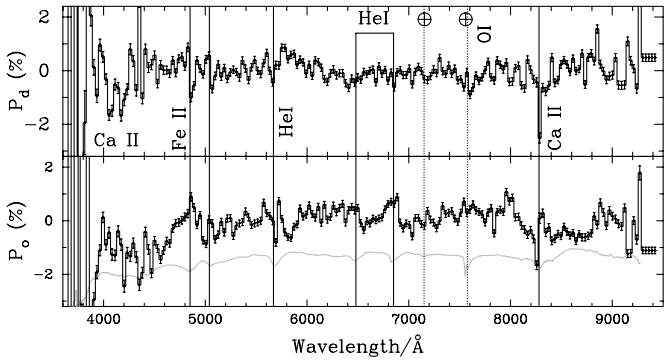

Figure 10. Spectropolarimetry of SN 2008D at 2008 February 15.18, projected onto the dominant (P_d; top panel) and orthogonal (P_o; bottom panel) axes. For comparison, the flux spectrum is plotted in gray in the bottom panel. Line identifications are those from Figure 3.

feature, but still imply that the polarization of O I is not as large as that observed for He I and Ca II.

4.2.6. Si II

At the first epoch the Si II feature is polarized, although with a peculiar polarization signature tracing the shallow line profile in the flux spectrum. At the absorption minimum (-7790 km s^{-1}) the corresponding polarization is 0.50%±0.15%. The maximum in polarization (0.73% ± 0.13%) actually occurs significantly redward of the minimum at 6260 Å (-4490 km s^{-1}). Following Malesani et al. (2009) and Modjaz et al. (2009; Section 3.1), this feature may be a blend of Si II and a HV component of Hα. If the polarization maximum is due to Hα, rather than Si II, it would imply that the absorption minimum of the Hα HV component has a velocity of $-17{,}050$ km s^{-1}. A similar shallow absorption profile was observed for SN 2005bf, although significant polarization was detected at the absorption minimum corresponding to Hα rather than Si II (Maund et al. 2007a).

As discussed in Section 3.1, the Si II feature is no longer apparent in the flux spectrum of the second epoch. In addition, we note that there is no significant signature in the polarization spectrum in the wavelength range where Si II is expected to lie, such that the feature has not been blended with another feature and instead it has disappeared at that time.

4.3. Decomposition of the Polarization

Following the scheme of Wang et al. (2001), the dominant axis of the data on the Stokes Q–U plane was determined by the weighted least-squares fit of a straight line to the data at both epochs. The angle α, between the polarization angle of the dominant axis and the Stokes Q axis were determined to be $40\overset{\circ}{.}2 \pm 1\overset{\circ}{.}4$ and $77\overset{\circ}{.}3 \pm 1\overset{\circ}{.}3$ at the first and second epochs, respectively. The dominant (P_d) and orthogonal (P_o) Stokes parameters were determined by rotating the data about the origin of the Stokes Q–U plane by an angle $-\alpha$, where

$$\begin{pmatrix} P_d \\ P_o \end{pmatrix} = \begin{pmatrix} \cos 2\alpha & \sin 2\alpha \\ -\sin 2\alpha & \cos 2\alpha \end{pmatrix} \begin{pmatrix} Q - Q_{\rm ISP} \\ U - U_{\rm ISP} \end{pmatrix}. \quad (2)$$

The determination of the polarization along and perpendicular to the dominant axis provides information on the principal asymmetry of the SN, and deviations from it (e.g., by the line-forming regions of particular species in the spectrum) and removes the effects of the position angle at which the SN was observed (although certain inclination effects remain). The spectropolarimetry projected into the dominant and orthogonal Stokes parameters is shown in Figures 9 and 10. In the case of SN 2008D, like SN 2002ap (Wang et al. 2003a), at both epochs the dominant axes were found to not pass through the origin of the Stokes Q–U plane, such that the presence of continuum polarization is observed as an offset in the orthogonal polarization component.

At the first epoch, Si II/Hα and He I lines are predominantly polarized along the dominant axis, whereas Ca II H&K and IR3 and the Fe II have components in both the dominant and orthogonal directions. A strong orthogonal polarization is observed close to the expected position of the O I λ7774 absorption.

At the second epoch the situation is reversed, with the He I lines being stronger in the orthogonal component. Despite the apparent decrease in the strength of the Fe II absorptions, these features are still present in the dominant component, although the strong feature observed in P_o is due to He I λ5015.

Caution is encouraged in interpreting the data on the dominant and orthogonal axes. The apparent shift of He I from the dominant axis (first epoch) to the orthogonal axis (second epoch) is primarily due to the apparent change in angle of the dominant axes ($\Delta\alpha \sim 37^\circ$) between the two epochs, due to the evolving flux and polarization of lines in the spectrum between the two epoch; as opposed to a bulk change in the polarization properties of the SN between the two epochs (such as observed for SN 2001ig; Maund et al. 2007b). Examination of the data on the Stokes Q–U plane in Figures 4 and 5 shows the data to be clustered in the same location at the two epochs.

As discussed in Section 4.4, the relative polarization of different species in the dominant and orthogonal directions indicates that, on the sky, the line-forming elements have very different distributions relative to each other within the ejecta.

4.4. The Polarization Angles of Absorption Features

The true power of spectropolarimetry, to study the shapes of SNe, is its ability to provide information of the geometry in the plane of the sky. Comparison of the degree of polarization and polarization angle against the velocities observed in the flux spectrum permits a three-dimensional tomographic analysis indicating the distribution of various elements within the ejecta in addition to the shape of the photosphere.

The polarization angles and velocities at absorption minimum for important lines in the spectrum are presented for both epochs in Figure 11. The polarization angle measured at the absorption

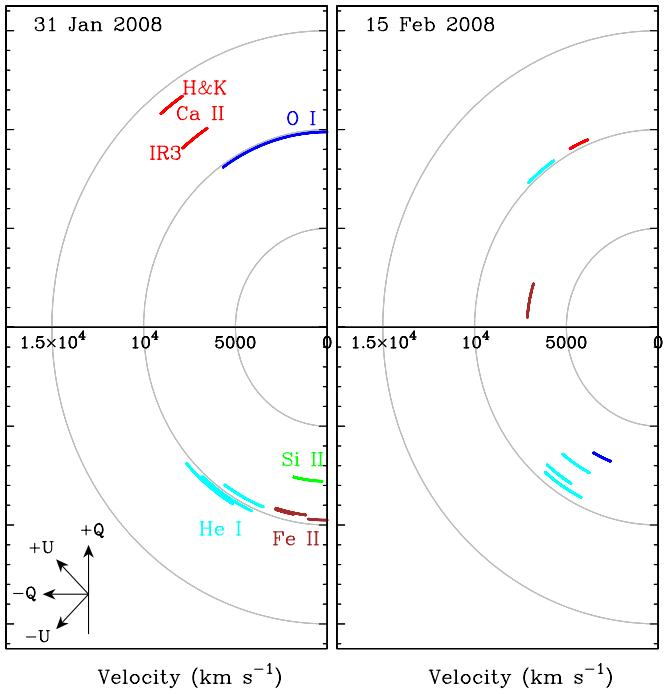

Figure 11. Polar plots showing the velocity and polarization angle at absorption minimum for Ca II H&K, He I λλ5015, 5876, 6678, 7065, Fe II (42), Si II λ6355, O I λ7774, and Ca II IR3 for the first and second observations of SN 2008D. The angle of each arc corresponds to the observed polarization angle on the sky (the arc length is $2\Delta\theta$) and the radius of the arc corresponds to the velocity. In this figure, north is up and east is left, with the corresponding orientation of the Stokes parameters indicated in the bottom left of the left panel.

(A color version of this figure is available in the online journal.)

minimum corresponds to the polarized component of continuum light that is *not* absorbed by the line-forming region, hence the approximate distributions of the various line-forming regions on the sky are rotated $\pi/2$ to the positions shown in Figure 11.

The observed polarization angle will be the result of mixing of polarized components from the continuum (if the photosphere is asymmetric) and the line's effective polarization (due to the shadow it casts on the photosphere). In the case of SN 2008D we have established, however, that the observed line polarization is significantly larger than the continuum polarization, and will dominate the measured polarization angle.

As shown in Figure 11, at the first epoch He I and Fe II are found in similar parts of the ejecta, with similar velocities (~ -10000 km s^{-1}), while the Si II λ6355 line is formed in a similar location, but at lower velocities. Both the Ca II H&K and IR3 lines have the same polarization angle, but are offset from the He I lines by $\Delta\theta = -100°$ (or +80°). This implies that there are, at least, two distinct ejecta components and that the Ca II lines, at much higher velocities, are disjoint from the rest of the ejecta.

At the second epoch, all velocities have decreased and Ca II and most of the He I lines are observed at approximately the same position angles as at the first epoch. The feature at λ5876 is separate from the other He I lines, with a polarization angle more consistent with Ca II. At this epoch, the He I λ5015 line is visible, and is grouped with the higher wavelength lines at λ6678, 7065. This suggests that the feature associated with λ5876 is actually a blend with Na ID (Wang et al. 2003a). Fe II (42) is observed at an intermediate polarization angle.

It is unclear at the first epoch, given the large degree of uncertainty, whether the O I line-forming region occupies a similar space to the Fe II line-forming region or if it is consistent with the Ca II region (due to the fact that a full rotation of the Stokes parameters occurs over only 180°). There is significant uncertainty in both the degree of polarization and polarization angle associated with O I due to coincidence with a strong telluric feature. As polarimetry measures differences in flux, the telluric absorption (assumed to be unpolarized) should not have any effect on the measured polarization, except for a reduction in the signal-to-noise ratio.

5. DISCUSSION

5.1. Spectropolarimetric Classification of SN 2008D

Following the classification scheme of Wang & Wheeler (2008), SN 2008D/XRF 080109 is classified as being of type D1+L(He I)+L(Ca II). This classification reflects the fact that a dominant axis can be fit to the data, although the polarization is better described as an ellipse on the Stokes Q–U plane. Furthermore, distinct loop features have been identified for He I and Ca II.

5.2. Comparison with Other Type Ibc SNe

SN 2008D shows a number of similarities and differences with the spectropolarimetry of other CCSNe, which can be used to compare and contrast likely geometries of these events. The intrinsic level of polarization of the continuum, dependent on the shape of the photosphere, is significantly detected but low, suggesting asymmetries of ∼10%. Similar low levels of continuum polarization have been observed over the range of Type Ibc SNe, including 2002ap, 2005bf, 2006aj, and 2007gr (Leonard et al. 2002; Kawabata et al. 2002; Wang et al. 2003a; Maund et al. 2007a, 2007c; Tanaka et al. 2008). The starkest contrast between these events is, however, the polarization associated with specific spectral lines.

For SN 2002ap, significant polarization associated with the O I λ7774 (0.9%; Wang et al. 2003a) and Ca II IR3 (Kawabata et al. 2002; Leonard et al. 2002) absorption components was observed. In that case, however, the progenitor star was a non-degenerate C/O star without He, whereas for SN 2008D the presence of a strong He I feature specifically implies the explosion of He-rich star (Soderberg et al. 2008; Modjaz et al. 2009). Maund et al. (2007a) interpreted the lack of polarization associated with O I in spectropolarimetry of the Type Ib SN 2005bf as indicating "shielding" of the O-rich core by the He envelope. On the other hand, 2007gr was a Type Ic SN, for which no He layer expected, which also showed little polarization associated with O I (Tanaka et al. 2008).

Modjaz et al. (2009) argue against using SN 2005bf as the comparison for SN 2008D on photometric and spectroscopic grounds, due to the double peaked light curve and the appearance of He I in the spectrum at 6 days prior to the second light curve maximum (∼34 days post-explosion). We note that the polarization properties of SN 2008D and SN 2005bf are actually quite similar. The loop feature for the He I λ5876 line for SN 2008D at the second epoch is similar to that observed for SN 2005bf (Maund et al. 2007a); except in this instance the signal-to-noise ratio is lower, making the loop less clear in Figure 6. Further similarity is observed for the resolved lines of Fe II in the flux spectrum, the low level of O I line polarization and the presence of Si II and HV Hα absorption features. Importantly, Ca II lines of both SN 2008D and 2005bf are observed to have minima at substantially higher velocities than He I, O I, and Fe II (see Figure 12) and are significantly polarized. This suggests that, at least for the second light curve maximum, SN 2005bf is

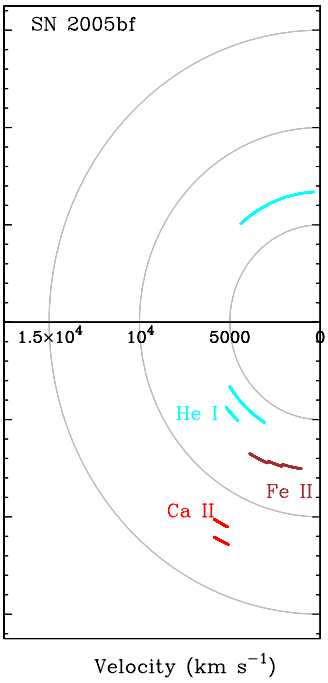

Figure 12. Polar plot of the polarization angles of particular spectral features from the observation of SN 2005bf at 6 days prior to second maximum (Maund et al. 2007a).

(A color version of this figure is available in the online journal.)

similar to SN 2008D at light curve maximum for the purposes of comparing their polarimetry and, ultimately, the natures of their explosions.

HV Ca components have proven quite common in Type Ia SNe (SN 2001el—Wang et al. 2003b; SN 2006X—Patat et al. 2009; Mazzali et al. 2005); here we note that they also seem rather common in SNIb/c as well. Spectropolarimetry has shown, however, that these features are highly polarized and that the polarization angles of these features are substantially different from the rest of ejecta.

5.3. Inferred Geometry of the Ejecta

Our spectropolarimetry of SN 2008D shows clear evidence that the ejecta are *chemically segregated*.

Figure 11 shows that the Ca II H&K and IR3 lines are formed at higher velocities than all the other spectral features studied in the spectrum. The He I lines all have approximately similar polarization angles at both epochs, except at the second epoch where one feature (λ5876) is observed to have a polarization close to that of Ca II.

The observed maximum polarizations for He I and Ca II, which exceed the theoretical limit for simple blocking of the unpolarized light, implies that the line-forming regions for these species are not distributed evenly across the photosphere. The HV components of the Ca II lines at both epochs, along with the significantly different polarization angle to the rest of the constituents of the ejecta, suggest the Ca II may be formed in a clump with a significant projected velocity along the line of sight. For SN 2007gr, Tanaka et al. inferred that the HV calcium was constrained in a bipolar distribution, with the other elements such as O I forming a torus in the orthogonal plane (due to the different polarization angles). Such a bipolar distribution of Ca II, for these Type Ibc SNe, may be related to the action of a jet-like flow. The low continuum polarization may indicate that the ejecta are viewed along, or close to, a principal axis of symmetry for the ejecta.

The presence of loop structures has been observed for nearly all CCSNe (Cropper et al. 1988; Wang et al. 2003b; Maund et al. 2007a) and some Type Ia SNe. These features have been interpreted by Kasen et al. (2003) and Maund et al. (2007a) as being due to the line-forming region, of the specific species, having an axial symmetry inclined with respect to the axial symmetry of the photosphere. This implies that there is no single global axial symmetry, and rather that the geometries of the ejecta are different for clumps of different species. If a single axial symmetry were present, then the data would be well described by a single dominant axis, and for SN 2008D it has been shown (see Section 4.3 and Figures 9 and 10) to not be the case.

The low level of continuum polarization determined here suggests the deviation of the photosphere from a spherical symmetry is low. This implies that the photosphere is receding through the ejecta at an approximately isotropic rate, which further suggests that the photosphere did not cross a significant change in the excitation structure between the two epochs of spectropolarimetry. In the cases of SNe 2004dj (Leonard et al. 2006), SN 2001ig (Maund et al. 2007b), and 2001dh (Maund et al. 2009), significant changes in the degree of polarization and the polarization angle with time implied depth-dependent geometry discontinuities. In the case of Type IIP and Type IIb SNe, such a significant change in polarization is expected once the photosphere crosses the chemical boundary between the H and He layers, where the photosphere can recede more quickly since He I is less ionized and, hence, presents less opacity than H. The geometry of He I is expected, therefore, to more closely match the underlying Ni distribution due to the asymmetric apparent luminosity of the photosphere (Höflich et al. 2001). Another such discontinuity is expected when the core products of nucleosynthesis and explosive burning are revealed, for which hydrodynamic simulations predict complex three-dimensional structures (Couch et al. 2009).

Gorosabel et al. (2008) observed small changes in the broadband polarization properties of SN 2008D over a larger time frame, from 2008 January 13 to 2008 March 28, which are consistent with our synthetic *V*-band polarimetry (see Section 3.2). While the true stability of the polarimetric standard adopted by Gorosabel et al., itself an SN, is debatable, the uncorrected polarimetry of SN 2008D shows only small variability. This implies that a significant geometry discontinuity was not just unobserved due to the paucity of our own observations. Our spectropolarimetry suggests, however, that while some of the variability may truly arise in the continuum, an additional factor that may contribute to the measured broadband polarization is evolving line polarization. The most important feature possibly affecting the *V*-band polarization is the He I/Na I feature, which is stronger, narrower and more polarized at the second epoch compared to the first. The striking absence of a discrete geometry discontinuity suggests that any axisymmetric structure directly associated with the explosion mechanism is not observed at the times of our observations or those of Gorosabel et al. (2008), and rather that the continuum polarization arises from only an elongation of the core, similar to that observed at early times for SN 2002ap (Wang et al. 2003a).

5.4. SN 2008D in the Jet-torus Paradigm

The apparent geometry of SN 2008D, at the two epochs, suggests the possibility of a jet-induced explosion. In the jet-torus

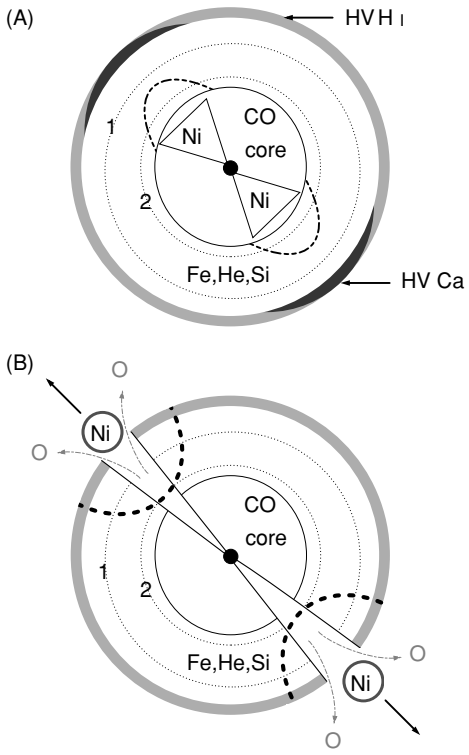

Figure 13. Possible scenarios, in the jet-torus paradigm, for the geometry of SN 2008D. The location of the HV line-forming regions is indicated by the light gray zone (and dark gray zones for Ca II). (A) Thermal energy dominated jet explosion. The jet elongates the core (heavy dashed line). HV Ca II and Hα features arise in a shell at the edge of the ejecta, with the high-velocity material aligned with the jet axis. He I, Si II, and Fe II occur in the main portion of the ejecta. The Ni-rich jets are contained within core, below the depth of the photosphere at the first and second epochs (dotted line). (B) Kinetic energy dominated jet explosion. Ni-rich material and other core-material, such as Ca II and O I, are transported to the surface. The outer edges of the ejecta are excited in the vicinity of the Ni-rich clumps (heavy black dotted lines). The position of the photosphere, at the two observational epochs, are indicated by light dotted lines.

explosion model, a jet-like flow propagates through the progenitor. Such a flow may originate from an asymmetry of neutrino deposition in the ejecta, the Standing Accretion Shock Instability (Blondin & Mezzacappa 2007) or a magnetorotational instability (Mikami et al. 2008). HV material is expected to arise from material impacted by the jet, while lateral shocks compress the main portion of the ejecta into a toroidal configuration (Khokhlov et al. 1999).

The lack of a detected geometry discontinuity is suggestive that either a jet-like flow had already been revealed at the time of our first observation or that it still remained shielded inside the core at the time of our second observation. The properties of jets which can either punch through the ejecta or stall within the core have been studied previously, and shown to be dependent on the relative mix of thermal and kinetic energy in the jet (Höflich et al. 2001; Couch et al. 2009). We propose two models (Scenarios A and B; schematic diagrams of these configurations are presented in Figure 13), in the jet-torus paradigm, which may have given rise to the spectropolarimetric properties. *Scenario A:* the jet-like flow (thermal energy dominated) stalled within the core. High-velocity Ca II is produced approximately along the direction of the jet-like flow, while the main portion of the ejecta exterior to the photosphere at both epochs (He I, Fe II, O I, and Si II) has a squashed spherical/toroidal geometry orthogonal to that of Ca II. Maund et al. (2007a) constructed a tilted jet model to explain the apparent lack of a single global axial symmetry for SN 2005bf. Similar to SN 2002ap (Wang et al. 2003a), the low degree of asymmetry of the photosphere is taken as an indication that such jets had not reached the height defined by the photosphere as measured at the epochs of the two observations. On the other hand the significant polarization associated with particular spectral features, with differing polarization angles for different species, is indicative of differing distributions of these elements within the ejecta, such that a single spherical symmetry is not appropriate. That loops are also observed for some spectral features is perhaps supportive of SN 2008D having a similar configuration as SN 2005bf, and a tilted axis of excitation with respect to the axis of symmetry of the photosphere. This may be evidence that there has not been full-scale transport of material that would have led to homogeneity, and that the elements reside in different portions of the ejecta. This scenario can be directly tested with observations at later epochs, when a large increase in the continuum polarization is expected as the asymmetric core layers, containing jet material, are revealed.

Scenario B: the jet-like flow (kinetic energy dominated) completely broke out of the progenitor prior to our first spectropolarimetric observation (and those of Gorosabel et al., at 18 days prior to our first observation), such that no discontinuity would be apparent as in the case of the jet stalling within the core. Such a scenario was suggested for SN 2002ap, where a polarization peak in the vicinity of O I λ7774/Ca II IR3 was interpreted as being due to light reflected by electrons in a high-velocity Ni-rich jet-like clump, exterior to the main ejecta, moving at $\gtrsim 0.115c$ (Leonard et al. 2002; Kawabata et al. 2002). Wang et al. (2003a) rejected this picture because (1) the polarization was associated with O I moving at $\sim$0.07c and (2) no features due to Ni or Co (in the range 1.6–1.8 μm) were present in the flux spectrum at early times, as would be expected if these radioactive elements had been deposited outside the main ejecta. For SN 2008D we note similarly that Modjaz et al. (2009) did not detect Ni or Co features in their IR spectra nor do we detect the asymmetric excitation of the ejecta illuminated by exterior Ni-rich clumps (with an obviously bipolar distribution). Similarly, the low degree of O I polarization, suggests there was little/no transport of core-material to the outer layers of the ejecta by the action of a jet-like flow.

We conclude that a jet-like flow, if present, stalled inside the CO core and, therefore, support Scenario A. An important consequence of Scenario A is, however, that the HV Ca II is *not* formed from products of nucleosynthesis from the progenitor, that was transported to the high-velocity (large radius) layer by a jet-like flow, rather it arose from primordial Ca abundance of the progenitor.

The question remains, however, as to the nature of the control mechanism which dictates why some Type Ibc SNe are associated with the GRB phenomenon and, hence, with highly energetic jets which penetrate to the exterior of the progenitor and others, such as SNe 2008D and 2005bf show evidence for jets which may have only remained in the core (Höflich et al. 2001).

5.5. Implications for the Shock-breakout Scenario

The suggestion from spectropolarimetric observations that any jet-like flows did not completely breakout has important implications for the interpretation of the X-ray emission of the associated XRF 080109.

In addition to our spectropolarimetry, Modjaz et al. (2009) report peculiar emission line profiles in late-time (91d after max.) nebular spectra of SN 2008D, at an epoch when the SN is optically thin, which is claimed to trace the asymmetric ejecta (see also Maeda et al. 2008). We note that our early-time spectropolarimetric observations of asymmetries in the distributions of a number of species within the ejecta are consistent with this picture (for example O I). At such late times, however, the ejecta can be shaped by a number of competing factors: the interaction between the circumstellar medium (CSM) and the ejecta and the evolution and interaction of physical processes (such as shocks and instabilities) over the lifetime of the SN. Importantly, at early times the measured geometry reflects the asymmetric nature of the explosion mechanism with little evolution from the moment of explosion. In this case, the observed geometry is more closely related to the geometry from which the early X-ray emission originated than the late-time observations of Modjaz et al. (2009) may be.

There are a number of open issues regarding the early X-ray emission from SN 2008D: whether it is due to thermal emission of shock breakout (Chevalier & Fransson 2008) or not (Soderberg et al. 2008; Xu et al. 2008; Li 2008); whether the emission is non-thermal (Soderberg et al.), a single blackbody (Chevalier & Fransson), or multiple blackbodies (Li); whether there is a dense wind surrounding the progenitor (Soderberg et al.) or not (Chevalier & Fransson); whether non-thermal emission arises from a shock-mediated Fermi acceleration (Soderberg et al.) or a variation of the forward/reverse shock paradigm of GRBs (Xu et al.). The common feature of these analyses is that they assume, or conclude, that the associated processes are spherically symmetric, or nearly so. Our spectropolarimetry data show that this is not the case, certainly by nearly maximum light when the observations are made, and presumably not as the shock is erupting from the surface of the star and propagating into any CSM.

Our observations do not directly constrain the geometry at breakout, but they give a strong caution that asymmetric shock breakout should be considered. Asymmetric shock breakout is unlikely to be accompanied by a single blackbody spectrum, so arguments that a single blackbody does not fit the X-ray spectrum are questionable. We also note that the X-ray spectrum softens considerably over the course of the X-ray outburst (Soderberg et al., supplemental material), so using the mean X-ray spectrum to characterize the physical nature of the outburst requires caution. Arguments that the X-ray burst cannot be a shock breakout (Xu et al.; Li) are subject to uncertainties in the color temperature compared to the effective temperature (Chevalier & Fransson), so must also be considered with caution. Given the concrete evidence for asymmetry and the likelihood that the shock erupted from restricted areas of the surface of the progenitor, all of these issues need to be reconsidered in the context of jet-like shock breakout.

6. CONCLUSIONS

SN 2008D has been observed to be significantly polarized at maximum and 2 weeks after maximum light. A significant amount of polarization is associated with the ISP, $p_{\rm ISP} = 1.2\%$ and $\theta_{\rm ISP} = 135^\circ \pm 4.^\circ 3$, arising in the host galaxy.

SN 2008D is intrinsically polarized, with a continuum polarization implying an asymmetry of the photosphere of $\lesssim 10\%$. Strong polarization associated with spectral lines shows evidence for significant asymmetries in the line-forming region of the ejecta above the photosphere. Loops on the Stokes Q–U plane are observed for lines of He I, in particular λ5876, and Ca II. A low level of polarization is potentially associated with O I λ7774, although this feature is complicated by blending with a strong telluric feature. Significant polarization is also observed for Fe II and Ca II; in the case of the latter, polarization of the highest velocity component of IR3 was measured to be $1.8\% \pm 0.3\%$ and $2.5\% \pm 0.7\%$ at the first and second epochs, respectively. The polarization of the Ca II IR3 feature shows a significantly different polarization angle, at both epochs, to other species in the spectrum, suggesting it arises in a different spatially distinct, higher-velocity portion of the ejecta than the lines of other species (i.e., the line-forming region for Ca II does not just lie at higher velocities than the line-forming regions of other species, but also with a different geometry).

The strong polarization associated with these lines suggests incomplete coverage of the photosphere by the line-forming regions for these species, and the differing polarization angles imply that the line-forming regions are different for different species. The absence of a strong polarization signature associated with O I λ7774, the absence of Ni or Co in early-time IR spectra, and a relatively low level of continuum polarization suggests no core material was transported to the outer layers of the ejecta by, for example, the action of a jet-like flow.

The observed asphericity of the photosphere (albeit at a relatively low level) and the chemically dependent structure of the line-forming regions above the photosphere demonstrates that SN 2008D was not spherically symmetric.

If SN 2008D was the result of a jet-induced explosion, then we conclude that the jet stalled within the core, causing the core and, hence, photosphere to become slightly elongated. The degree of elongation is observed to change as a function of depth over the period of our spectropolarimetry and over the period for which broadband polarimetry has also been reported. In terms of spectropolarimetry, SN 2008D is found to be closely related to SN 2005bf (albeit at 6 days before the second light curve maximum of the latter). The spectropolarimetric study of the geometries of SN 2002ap, 2005bf, and 2008D is shown to be consistent within the jet-torus paradigm, but in which the jet remains within the cores of the progenitor. We hypothesize that relatively late-time polarimetric observations of CCSNe, before the optical depth to electron scattering drops below unity, will reveal a geometry discontinuity consistent with the photosphere having reached the position of a stalled jet.

The observation of asymmetries of SN 2008D at early times has important implications for the study of the X-ray and UV shock breakout and the assumption of spherical symmetry.

The research of J.R.M. is funded through the Sophie & Tycho Brahe Fellowship. The Dark Cosmology Centre is supported by the DNRF. The research of J.C.W. is supported in part by NSF grant AST-0707769. The authors are grateful to the European Organisation for Astronomical Research in the Southern Hemisphere for the generous allocation of observing time. They especially thank the staff of the Paranal Observatory for their competent and never-tiring support of this project in service mode.

REFERENCES

Appenzeller, I., et al. 1998, Messenger, 94, 1
Berger, E., & Soderberg, A. M. 2008, GRB Coordinates Network, 7159
Blondin, J. M., & Mezzacappa, A. 2007, Nature, 445, 58
Chandrasekhar, S. 1960, Radiative Transfer (New York: Dover)
Chevalier, R. A., & Fransson, C. 2008, ApJ, 683, L135
Couch, S. M., Wheeler, J. C., & Milosavljevic, M. 2009, ApJ, 696, 953

Cropper, M., Bailey, J., McCowage, J., Cannon, R. D., & Couch, W. J. 1988, MNRAS, 231, 695
Gorosabel, J., et al. 2008, arXiv:0810.4333
Höflich, P. 1991, A&A, 246, 481
Höflich, P., Gerardy, C. L., Marion, H., & Quimby, R. 2006, New Astron. Rev., 50, 470
Höflich, P., Khokhlov, A., & Wang, L. 2001, in AIP Conf. Ser. 586, 20th Texas Symposium on Relativistic Astrophysics, ed. J. C. Wheeler & H. Martel (Melville, NY: AIP), 459
Howell, D. A., Höflich, P., Wang, L., & Wheeler, J. C. 2001, ApJ, 556, 302
Jeffery, D. J. 1991, ApJS, 77, 405
Kasen, D., et al. 2003, ApJ, 593, 788
Kawabata, K. S., et al. 2002, ApJ, 580, L39
Khokhlov, A. M., Höflich, P. A., Oran, E. S., Wheeler, J. C., Wang, L., & Chtchelkanova, A. Y. 1999, ApJ, 524, L107
Leonard, D. C., & Filippenko, A. V. 2001, PASP, 113, 920
Leonard, D. C., Filippenko, A. V., Ardila, D. R., & Brotherton, M. S. 2001, ApJ, 553, 861
Leonard, D. C., Filippenko, A. V., Chornock, R., & Foley, R. J. 2002, PASP, 114, 1333
Leonard, D. C., et al. 2006, Nature, 440, 505
Li, L.-X. 2008, MNRAS, 388, 603
Li, W., & Filippenko, A. V. 2008, Central Bureau Electronic Telegrams, 1202
Maeda, K., et al. 2008, Science, 319, 1220
Malesani, D., et al. 2009, ApJ, 692, L84
Maund, J. R. 2008, A&A, 481, 913
Maund, J., Wheeler, J., Patat, F., Baade, D., Wang, L., & Höflich, P. 2007a, MNRAS, 381, 201
Maund, J., Wheeler, J., Patat, F., Wang, L., Baade, D., & Höflich, P. 2007b, ApJ, 671, 1944
Maund, J. R., Wheeler, J. C., Patat, F., Baade, D., Wang, L., & Höflich, P. 2007c, A&A, 475, L1
Maund, J. R., Wheeler, J. C., Patat, F., Wang, L., & Höflich, P. A. 2009, submitted
Mazzali, P. A., et al. 2005, ApJ, 623, L37
Mazzali, P. A., et al. 2008, Science, 5893, 1185
Mikami, H., Sato, Y., Matsumoto, T., & Hanawa, T. 2008, ApJ, 683, 357
Modjaz, M., et al. 2009, ApJ, 702, 226
Patat, F., Baade, D., Höflich, P. A., Maund, J. R., Wang, L., & Wheeler, J. C. 2009, A&A, in press (arXiv:0909.5564)
Scarrott, S. M., Ward-Thompson, D., & Warren-Smith, R. F. 1987, MNRAS, 224, 299
Schlegel, D. J., Finkbeiner, D. P., & Davis, M. 1998, ApJ, 500, 525
Serkowski, K., Mathewson, D. L., & Ford, V. L. 1975, ApJ, 196, 261
Soderberg, A. M., et al. 2008, Nature, 453, 469
Tanaka, M., Kawabata, K. S., Maeda, K., Hattori, T., & Nomoto, K. 2008, ApJ, 689, 1191
Tanaka, M., et al. 2009, ApJ, 692, 1131
Thöne, C. C., Michalowski, M. J., Leloudas, G., Cox, N. L. J., Fynbo, J. P. U., Sollerman, J., Hjorth, J., & Vreeswijk, P. M. 2009, ApJ, 698, 1307
Tran, H. D., Filippenko, A. V., Schmidt, G. D., Bjorkman, K. S., Jannuzi, B. T., & Smith, P. S. 1997, PASP, 109, 489
Wang, L., Baade, D., Höflich, P., & Wheeler, J. C. 2003a, ApJ, 592, 457
Wang, L., Howell, D. A., Höflich, P., & Wheeler, J. C. 2001, ApJ, 550, 1030
Wang, L., & Wheeler, J. C. 2008, ARA&A, 46, 433
Wang, L., et al. 2003b, ApJ, 591, 1110
Xu, D., Zou, Y.-C., & Fan, Y.-Z. 2008, arXiv:0801.4325